Si-Wei Chen · Xue-Song Wang
Shun-Ping Xiao · Motoyuki Sato

Target Scattering Mechanism in Polarimetric Synthetic Aperture Radar

Interpretation and Application

Springer

Target Scattering Mechanism in Polarimetric Synthetic Aperture Radar

Si-Wei Chen · Xue-Song Wang
Shun-Ping Xiao · Motoyuki Sato

Target Scattering Mechanism in Polarimetric Synthetic Aperture Radar

Interpretation and Application

Springer

Si-Wei Chen
State Key Laboratory of Complex
Electromagnetic Environment Effects on
Electronics and Information System
National University of Defense Technology
Changsha, Hunan
China

Xue-Song Wang
State Key Laboratory of Complex
Electromagnetic Environment Effects on
Electronics and Information System
National University of Defense Technology
Changsha, Hunan
China

Shun-Ping Xiao
State Key Laboratory of Complex
Electromagnetic Environment Effects on
Electronics and Information System
National University of Defense Technology
Changsha, Hunan
China

Motoyuki Sato
Center for Northeast Asian Studies
Tohoku University
Sendai
Japan

ISBN 978-981-10-7268-0 ISBN 978-981-10-7269-7 (eBook)
https://doi.org/10.1007/978-981-10-7269-7

Library of Congress Control Number: 2017959905

Printed on acid-free paper

This Springer imprint is published by the registered company Springer Nature Singapore Pte Ltd.
part of Springer Nature
The registered company address is: 152 Beach Road, #21-01/04 Gateway East, Singapore 189721, Singapore

Preface

Microwave remote sensor can work day and night, and is nearly unaffected by weather and atmospheric conditions. It plays a more and more important role for earth and other planet monitoring in both global and regional scales. As an imaging system, polarimetric synthetic aperture radar (PolSAR) has the ability to obtain fully polarimetric information and becomes one of the mainstreams in microwave remote sensing. Full polarization acquisition greatly enhances radar capability in many aspects and expands its application fields. The studies and applications of polarimetric radar imaging enter a golden era with the significant supports of solid radar polarimetry theory, advanced signal processing techniques, and easily accessible high-quality data sets. Credits are owed to those radar polarimetry pioneers in both fundamental theory and hardware system development.

Based on giants' shoulders, this book focuses on a branch of radar polarimetry and PolSAR studies: interpretation and application of target scattering mechanism in PolSAR. This research branch is dedicated to bridge the gap between the acquired data and practical applications. Also, it is one of the main challenges in polarimetric radar imaging. This book mainly summarizes our studies, researches, and thoughts of this field in the past decade. Hopefully, it will be benefit for potential readers. This book mainly contains five chapters.

Chapter 1 briefly reviews the basic theories in radar polarimetry, the fundamental principles in polarimetric radar imaging, and some advanced concepts for understanding and interpreting target scattering mechanisms.

Chapter 2 focuses on advanced polarimetric target decomposition development mainly in terms of model-based decomposition. The limitations of classical model-based decomposition are firstly discussed. Meanwhile, a review of recent advances in scattering mechanism modeling and decomposition theorem is presented. Then, a polarimetric-interferometric model-based decomposition is introduced, which is one of several first attempts to fuse both polarimetric and interferometric information to enhance the target decomposition performance. Besides, a general model-based decomposition scheme, which uses all elements of a polarimetric coherency matrix, is presented. The key principles and features include: the double- and odd-bounce scattering models are generalized with their

independent orientation angles; each scattering model is considered with equal weight and without any implied assumption of model priority; the unknown model parameters are optimally and simultaneously determined; the occurrence of negative power is theoretically avoided. In addition, the reflection symmetry assumption, branch conditions, and manual interventions are also avoided. Further perspectives for future developments are also discussed.

Chapter 3 introduces the uniform polarimetric matrix rotation theory which aims to investigate target scattering orientation diversity. The underlining physics is that target scattering responses are generally orientation dependent. Although this orientation dependency effect usually leads to scattering mechanism ambiguity and makes PolSAR data modeling and interpretation difficult, target scattering orientation diversity also contains rich information which is seldom considered and explored. Proper exploration of such orientation diversity has the potential to provide valuable insights to reveal intrinsic properties of different targets. The concept of the rotation domain along the radar line of sight is introduced. The core idea is to extend polarimetric matrix at a given imaging geometry to the rotation domain. Then, the uniform representation of each polarimetric matrix element and a new set of oscillation parameters in the rotation domain are derived and summarized. Application demonstrations in terms of land cover classification are carried out.

Chapter 4 introduces the visualization and characterization tool of polarimetric coherence pattern. Complementary to the uniform polarimetric matrix rotation theory introduced in Chap. 3, the developed polarimetric coherence pattern provides solutions to mine and characterize the hidden information between two arbitrary polarimetric channels. A set of new polarimetric features are derived to completely represent those hidden information. Land cover classifications demonstrate the efficiency of these polarimetric features. Furthermore, polarimetric coherence enhancement in the rotation domain is investigated and demonstrated for manmade target extraction and crops discrimination.

Chapter 5 focuses on natural disaster damage investigation by exploring multi-temporal PolSAR data using fully polarimetric techniques. The study case is the great tsunami induced by the earthquake of March 11, 2011, which occurred beneath the Pacific off the northeastern coast of Japan. Two authors, Si-Wei Chen and Motoyuki Sato, experienced this destructive disaster and carried out field investigations afterward. In this chapter, the polarimetric scattering mechanism changes pre- and post-event are examined in theory and confirmed by advanced model-based decomposition and polarization orientation angle techniques. Then, damage indexes are proposed and their relationships to real damage levels are disclosed and established. A rapid urban damage level mapping technique is developed therein which has the capability to simultaneously and automatically identify urban damage locations and damage levels for a huge monitoring area. Finally, other damage condition investigations in terms of flooded river area and flooded paddy field are also carried out.

Finally, limited by our knowledge, experience, and time, there may be some unavoidable mistakes. Looking forward to readers' suggestions and comments.

Changsha, China — Si-Wei Chen
Changsha, China — Xue-Song Wang
Changsha, China — Shun-Ping Xiao
Sendai, Japan — Motoyuki Sato
October 2017

Acknowledgements

During our studies and researches, we received great and uncountable help and support from a number of colleagues, researchers, and students. Here, we would like to express our deep gratitude and thanks to Prof. Wolfgang-Martin Boerner, University of Illinois, USA; Dr. Jong-Sen Lee and Dr. Thomas L. Ainsworth, Naval Research Laboratory, USA; Prof. Yoshio Yamaguchi, Niigata University, Japan; Dr. Ridha Touzi, Natural Resources Canada, Canada; Dr. Jakob J. van Zyl, Jet Propulsion Laboratory, USA; Prof. Jian Yang, Tsinghua University, China; Dr. Konstantinos P. Papathanassiou, German Aerospace Center, Germany; Dr. Masanobu Shimada and Mr. Masato Ohki, Japan Aerospace Exploration Agency, Japan; Dr. Zheng-Shu Zhou, Commonwealth Scientific and Industrial Research Organisation, Australia; Prof. Shunichi Koshimura, Tohoku University, Japan, and so on.

Also, our studies and researches cannot be accomplished without the support of valuable data sets. We would like to sincerely thank Japan Aerospace Exploration Agency for providing the ALOS-1 and ALOS-2 data; National Institute of Information and Communications Technology for providing Pi-SAR and Pi-SAR2 data; European Space Agency and German Aerospace Center for providing E-SAR and F-SAR data; Jet Propulsion Laboratory for providing the AIRSAR and UAVSAR data. These valuable and high-quality data sets greatly support our researches and make our ideas come true.

The research work presented in this book was carried out at the State Key Laboratory of Complex Electromagnetic Environment Effects on Electronics and Information System (CEMEE), School of Electronic Science, National University of Defense Technology, Changsha, China, and the Center for Northeast Asian Studies, Tohoku University, Sendai, Japan. These researches were supported in part by the National Natural Science Foundation of China (NSFC) under Grants "Ultra-high-resolution polarimetric SAR manmade target interpretation and three-dimensional reconstruction" (no. 61771480), "Building earthquake damage evaluation based on scattering mechanism investigation using polarimetric SAR data" (no. 41301490), and "Fundamental theory and key technology of radar

polarimetry" (no. 61490690) and were also supported in part by the Japan Society for the Promotion of Science (JSPS) Grant-in-Aid for Scientific Research (A) 23246076. The authors sincerely acknowledge all these significant supports.

We also thank the Institute of Electrical and Electronics Engineers (IEEE) for the permission to reuse our materials that have appeared in IEEE publications; the Taylor & Francis for the permission to reuse our materials that have appeared in its publication; the Institute of Electronics, Information and Communication Engineers (IEICE) for the permission (no. 17RA0074) to reuse our materials that have appeared in an IEICE publication.

October 2017

Si-Wei Chen
Xue-Song Wang
Shun-Ping Xiao
Motoyuki Sato

Contents

1 Fundamentals of Polarimetric Radar Imaging and Interpretation 1
1.1 Radar Polarimetry Basics 2
1.1.1 Polarization of Electromagnetic Wave 2
1.1.2 Polarimetric Scattering Matrix 5
1.1.3 Polarization Basis Transformation 6
1.1.4 Polarimetric Coherency Matrix in Linear Polarization Basis 7
1.1.5 Polarimetric Covariance Matrix in Linear Polarization Basis 8
1.1.6 Polarimetric Covariance Matrix in Circular Polarization Basis 9
1.2 Polarimetric Radar Imaging 10
1.2.1 SAR Overview 10
1.2.2 SAR Imaging Principles 11
1.2.3 PolSAR Principles 13
1.2.4 InSAR Principles 16
1.2.5 PolInSAR Principles 19
1.3 Target Scattering Mechanism Interpretation Overview 22
1.3.1 Basic Eigenvalue–Eigenvector-Based Decomposition 24
1.3.2 Basic Model-Based Decomposition 27
1.3.3 Polarization Orientation Angle and Orientation Compensation 34
1.4 Summary 38
References 38

2 Advanced Polarimetric Target Decomposition 43
2.1 Introduction 43
2.2 Limitations of Classical Model-Based Decomposition 44
2.2.1 Dynamic Range of Volume Scattering Component 44
2.2.2 Orientation Compensation and Its Limitation 47

2.3 Recent Advances in Model-Based Decomposition 55
2.3.1 Orientation Compensation Processing 56
2.3.2 Nonnegative Eigenvalue Constraint 59
2.3.3 Generalized Volume Scattering Models 59
2.3.4 Generalized Double- and Odd-Bounce Scattering Models 60
2.3.5 Complete Information Utilization 60
2.3.6 Full-Parameter Inversion Strategy 61
2.3.7 Fusion of Polarimetric-Interferometric Information 62
2.4 Adaptive Polarimetric-Interferometric Model-Based Decomposition 62
2.4.1 PolInSAR Coherence Diversity Investigation 63
2.4.2 Adaptive Model-Based Decomposition Development 66
2.4.3 Experiment with Airborne PolInSAR Data 70
2.4.4 Experiment with Spaceborne PolInSAR Data 75
2.4.5 Discussions and Perspectives 79
2.4.6 Brief Summary 80
2.5 General Model-Based Decomposition 80
2.5.1 General Decomposition Scheme 81
2.5.2 Experimental Results and Analysis 85
2.5.3 Further Analysis 91
2.5.4 Brief Summary 98
2.6 Discussions and Perspectives 99
2.6.1 PolSAR Data Preprocessing Issue 99
2.6.2 Radar Frequency Issue 99
2.6.3 High Spatial Resolution Issue 99
2.6.4 Model Priority Issue 100
2.6.5 Solution Stability 100
2.6.6 Performance Evaluation Issue 101
2.6.7 Further Generalized Modeling 102
2.7 Conclusion 102
References 103

3 Uniform Polarimetric Matrix Rotation Theory 107
3.1 Introduction 107
3.2 Polarimetric Matrix in Rotation Domain 108
3.2.1 Polarimetric Scattering Matrix in Rotation Domain 108
3.2.2 Polarimetric Coherency Matrix in Rotation Domain 109
3.2.3 Cascade Rotation Property 110
3.2.4 Roll-Invariant Terms 111
3.3 Development of the Uniform Polarimetric Matrix Rotation Theory 112
3.3.1 Uniform Representation 112
3.3.2 Interpretation of Oscillation Parameters 113

3.3.3 Further Derived Angle Parameters and Interpretation 116
3.3.4 Links to Huynen Parameters and Interpretation 119
3.3.5 Polarimetric Covariance Matrix in Rotation Domain 120
3.4 Demonstration and Application of Oscillation Parameters 122
3.4.1 Multi-Frequency Pi-SAR Data Description 123
3.4.2 Oscillation Parameters 123
3.5 Demonstration and Application of Angle Parameters 126
3.5.1 Multi-Frequency AIRSAR Data Description 126
3.5.2 Angle Parameters 127
3.5.3 Unsupervised Land Cover Classification 128
3.6 Supervised Classification Demonstration 131
3.6.1 Demonstration with SVM Classifier 132
3.6.2 Demonstration with DT Classifier 135
3.7 Discussions and Perspectives 137
3.7.1 Summary of Roll-Invariant Terms 137
3.7.2 Utilization Perspectives 137
3.8 Conclusion 138
References 139

4 Polarimetric Coherence Pattern: A Visualization and Interpretation Tool 143
4.1 Introduction 143
4.2 Polarimetric Coherence Pattern 144
4.2.1 Definition of Polarimetric Coherence Pattern 144
4.2.2 Visualization and Characterization 145
4.2.3 Interpretation and Discussion 147
4.2.4 Demonstration and Investigation 149
4.3 Classification Development and Application 155
4.3.1 Classification Methodology Development 155
4.3.2 Classification with UAVSAR PolSAR Data 157
4.3.3 Classification with AIRSAR PolSAR Data 157
4.3.4 Discussions and Perspectives 160
4.4 Further Application for Manmade Target Extraction 162
4.4.1 Polarimetric Coherence Enhancement Over Urban Area . . . 163
4.4.2 Manmade Target Extraction 165
4.5 Further Application for Crops Discrimination 167
4.5.1 Polarimetric Coherence Enhancement Over Crop Area 169
4.5.2 Feature Selection and Crops Discrimination 171
4.6 Conclusions 177
References 178

5 Natural Disaster Investigation and Urban Damage Level Mapping 181
5.1 Introduction 181
5.2 Urban Damage Characterization Using Polarimetric Technique . . . 182
5.2.1 Study Area and Data Description 183
5.2.2 Model-Based Decomposition Technique 186
5.2.3 Polarization Orientation Angle Technique 193
5.3 Urban Damage Level Mapping 200
5.3.1 Urban Area Extraction 202
5.3.2 Damage Level Index Estimation 205
5.3.3 Experimental Study and Demonstration 205
5.4 Other Damage Situations Investigation 214
5.4.1 Flooded River Area Analysis Using Spaceborne PolSAR Data 214
5.4.2 Flooded Paddy Field Analysis Using Airborne PolSAR Data 217
5.5 Conclusion 222
References 223

Chapter 1
Fundamentals of Polarimetric Radar Imaging and Interpretation

Radar is a system that transmits and receives electromagnetic wave for the detection and location of reflecting objects. The terminology **radar** originally comes from the words ***ra***dio ***d***etection ***a***nd ***r***anging [1]. With the progresses and advances in hardware technologies and signal processing theories, the definition and function of radar have been greatly expanded. Modern radar can generate a radar image to "see" target directly.

Polarization is an intrinsic property of the electromagnetic wave [2]. Researches on polarization have a long history since the seventeenth century, while the discovery of the polarization phenomenon was even earlier about A.D. 1000 [3]. However, the earliest work on radar polarimetry only dates back to the 1940s. Many pioneers dedicated to this field and stimulated the development of radar polarimetry. In 1945, G. W. Sinclair introduced the scattering matrix to link the transmitted and received waves in Jones vectors and to represent the fully polarimetric information scattered by a coherent scatterer [4]. It is also known as the Sinclair scattering matrix. Later, E. M. Kennaugh proposed the theory of the optimal polarization in the early 1950s by demonstrating that there are characteristic polarization states leading to the maximum or minimum receiving power [5]. Meanwhile, the Kennaugh matrix and Mueller matrix which link the associated Stokes vectors were also presented [5, 6]. Besides, the concept of the power scattering matrix, which is suitable to optimize the density of the scattering field, has been proposed by C. D. Graves [7]. Until the work of J. R. Huynen [8, 9], radar polarimetry experienced a depression with only a few notable achievements. Huynen's dissertation [8] opened a new stage for radar polarimetry in 1970 and reattracted more interests and attentions. However, the full understanding of the importance of radar polarimetry was limited by the lack of advanced polarimetric radar systems. In 1970s and early 1980s, the major contributions were from W. M. Boerner who first rediscovered and pointed out the importance of polarization in electromagnetic scattering. He enhanced the work from the E. M. Kennaugh and J. R. Huynen and extended the optimal polarization theory [10–12].

S.-W. Chen et al., *Target Scattering Mechanism in Polarimetric Synthetic Aperture Radar*, https://doi.org/10.1007/978-981-10-7269-7_1

More detailed reviews of the historical development of radar polarimetry can be found in [13]. With these pioneers' hard efforts, the theory framework of radar polarimetry has been established and reviewed in [14–16]. Besides, the studies on the processing of wideband polarization information and further extensions of optimal polarization theory can be found in [17–19]. With the advances in hardware systems, signal processing techniques, and interpretation theories, radar polarimetry has been developed rapidly and has become a key technique in microwave remote sensing.

Microwave remote sensor, which can work day and night, and is nearly unaffected by weather and atmospheric conditions, plays a more and more important role for the earth and other planet monitoring in both global and regional scales. As an imaging system, polarimetric synthetic aperture radar (PolSAR) is one of the mainstreams in microwave remote sensing. It can obtain fully polarimetric information by transmitting and receiving microwaves with specific polarization states. Fully polarimetric information is sensitive to scattering mechanisms related to target responses during backscattering procedure. Full polarization acquisition can enhance radar capability in scattering mechanism understanding, target parameters (e.g., material, shape, and orientation) retrieval, and so on. In this vein, many current airborne and spaceborne SAR systems are equipped with full polarization mode. Huge amount of PolSAR data sets have been acquired by these systems especially the routinely operated spaceborne systems such as on-orbit Radarsat-2 from Canada, TerraSAR from Germany, ALOS-2 from Japan, GaoFen-3 from China. These valuable data sets greatly stimulate the studies in both theory and application. Scattering mechanism understanding is a bridge between the collected data and real applications. Generally, scattering mechanisms are determined by a set of factors such as radar frequency, radar bandwidth, illumination direction, target dielectric/geometric properties. Although the basic theory of radar polarimetry has been well established, scattering mechanism modeling and interpretation are still ongoing. How to effectively extract robust and useful information from collected data is still challenging.

1.1 Radar Polarimetry Basics

1.1.1 Polarization of Electromagnetic Wave

The fundamental theory of electromagnetic fields is based on Maxwell's equations [2]

$$\begin{aligned} \nabla \times \boldsymbol{E} &= -\frac{\partial \boldsymbol{B}}{\partial t} \quad \nabla \times \boldsymbol{H} = J + \frac{\partial \boldsymbol{D}}{\partial t} \\ \nabla \cdot \boldsymbol{B} &= 0 \qquad \nabla \cdot \boldsymbol{D} = \boldsymbol{\rho}_v \end{aligned} \tag{1.1.1}$$

where $\boldsymbol{E}$, $\boldsymbol{H}$, $\boldsymbol{B}$, and $\boldsymbol{D}$ are the wave electric field, magnetic field, electric induction, and magnetic induction, respectively. J and ρ_v are electric current density and electric charge density, respectively.

For time-harmonic fields at a single frequency $\omega = 2\pi f$, $\boldsymbol{E}$ and $\boldsymbol{H}$ at an arbitrary position r can be expressed as

$$\boldsymbol{E} = \boldsymbol{E}(r)\exp(j\omega t) \qquad \boldsymbol{H} = \boldsymbol{H}(r)\exp(j\omega t) \tag{1.1.2}$$

Assuming that electromagnetic fields are generated in free space by sources J and ρ_v in a local region where $J = 0$ and $\rho_v = 0$ for fields out of this region, then Maxwell's equations become

$$\begin{array}{ll} \nabla \times \boldsymbol{E} = -j\omega B & \nabla \times \boldsymbol{H} = j\omega D \\ \nabla \cdot \boldsymbol{B} = 0 & \nabla \cdot \boldsymbol{D} = 0 \end{array} \tag{1.1.3}$$

Besides, the free-space constitutive relations are

$$\boldsymbol{D} = \varepsilon_0 \boldsymbol{E} \qquad \boldsymbol{B} = \mu_0 \boldsymbol{H} \tag{1.1.4}$$

where ε_0 and μ_0 are the dielectric permittivity and magnetic permeability for free space.

Substituting the (1.1.3) and (1.1.4) into $\nabla \times (\nabla \times \boldsymbol{E}) = \nabla(\nabla \cdot \boldsymbol{E}) - \nabla^2 \boldsymbol{E}$, the wave equations can be obtained

$$\nabla^2 \boldsymbol{E} + \mathrm{k}^2 \boldsymbol{E} = 0 \qquad \nabla^2 \boldsymbol{H} + \mathrm{k}^2 \boldsymbol{H} = 0 \tag{1.1.5}$$

where k is the wavenumber and $k^2 = \omega^2 \mu_0 \varepsilon_0$.

Generally, the vector $\boldsymbol{E}$ of a time-harmonic electromagnetic wave varies sinusoidally with time at a fixed point in space. The polarization of the wave is described by the locus of the tip of the vector $\boldsymbol{E}$ as time progresses. For plane wave, the electric and magnetic fields are perpendicular to each other, and both are perpendicular to the wave propagation direction. If this plane wave propagates along the positive z-direction, the electric field $\boldsymbol{E}$ in (1.1.5) becomes

$$\frac{\partial^2 \boldsymbol{E}(z,t)}{\partial z^2} + k^2 \boldsymbol{E}(z,t) = 0 \tag{1.1.6}$$

The real components of the instantaneous electric field of the solution for (1.1.6) along x and y axes are

$$\boldsymbol{E}(z,t) = \begin{bmatrix} \boldsymbol{E}_x(z,t) \\ \boldsymbol{E}_y(z,t) \end{bmatrix} = \begin{bmatrix} a_x \cos(\omega t - kz + \phi_x) \\ a_y \cos(\omega t - kz + \phi_y) \end{bmatrix} \tag{1.1.7}$$

where a_x and a_y denote the magnitudes, while ϕ_x and ϕ_y denote the phases for x and y components, respectively.

At a specific position $z = z_0$, the temporal wave trajectory is determined

$$\left[\frac{\boldsymbol{E}_x(z_0,t)}{a_x}\right]^2 - 2\frac{\boldsymbol{E}_x(z_0,t)\boldsymbol{E}_y(z_0,t)}{a_x a_y}\cos\phi + \left[\frac{\boldsymbol{E}_y(z_0,t)}{a_y}\right]^2 = \sin^2\phi a_x \tag{1.1.8}$$

where $\phi = \phi_y - \phi_x$ is the phase difference.

In the most cases, the expression in (1.1.8) is the equation of an ellipse and describes the elliptical polarization. When $\phi = 0$ or $\phi = \pm\pi$, the ellipse shrinks to a line which indicates the linear polarization. When $\phi = \pm\frac{\pi}{2}$ and $\frac{a_x}{a_y} = 1$, the ellipse becomes a circle which represents the circular polarization.

Generally, the locus of (1.1.8) has been named as the polarization ellipse to describe the wave polarization. The shape of polarization ellipse can be characterized by three parameters, shown in Fig. 1.1.

- A is the ellipse amplitude and determined as

$$A = \sqrt{a_x^2 + a_y^2} \tag{1.1.9}$$

- $\theta \in \left[-\frac{\pi}{2}, \frac{\pi}{2}\right]$ is the ellipse orientation and is defined as the angle between the major axis of the ellipse and the x-axis, expressed as

$$\tan 2\theta = 2\frac{a_x a_y}{a_x^2 - a_y^2}\cos\phi \tag{1.1.10}$$

- $|\tau| \in \left[0, \frac{\pi}{4}\right]$ is the ellipticity and defined as

$$|\sin 2\tau| = 2\frac{a_x a_y}{a_x^2 + a_y^2}|\sin\phi|. \tag{1.1.11}$$

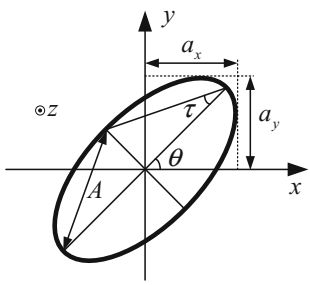

Fig. 1.1 Polarization ellipse

1.1.2 Polarimetric Scattering Matrix

For radar, the transmitted electromagnetic wave will interact with a potential target when the wave reaches it. During the interaction, part of the energy carried by the incident wave is absorbed by the target while the rest is reradiated as a new electromagnetic wave and modulated with the properties of the target itself. In order to characterize the target property from the viewpoint of power exchange, for point target which is smaller than the footprint of the radar system, the radar cross-section (RCS) σ is introduced [1]

$$\sigma = 4\pi r^2 \frac{|\boldsymbol{E}_\mathrm{S}|^2}{|\boldsymbol{E}_\mathrm{I}|^2} \tag{1.1.12}$$

where $\boldsymbol{E}_\mathrm{I}$ is the incident electromagnetic wave reaching the target, $\boldsymbol{E}_\mathrm{S}$ is the scattered wave reradiated by the same target, r is the distance between the radar and the target.

For extended or distributed target, which is larger than the footprint of the radar system, the scattering coefficient σ^0 is defined [1]

$$\sigma^0 = \frac{\langle\sigma\rangle}{A_0} = \frac{4\pi r^2}{A_0} \frac{\left\langle |\boldsymbol{E}_\mathrm{S}|^2 \right\rangle}{|\boldsymbol{E}_\mathrm{I}|^2} \tag{1.1.13}$$

Scattering coefficient σ^0 is the averaged RCS per unit area A_0 and represents the ratio of the statistically averaged scattered power density to the average incident power density over the surface of the sphere with radius r.

Generally, the RCS σ and scattering coefficient σ^0 carry the intrinsic information of the scatterers and targets, such as the dielectric properties, geometric structures. Fully polarimetric radar can obtain additional polarimetric information of targets by transmitting and receiving orthogonal electromagnetic waves. The polarization of a plane and monochromatic electromagnetic wave can be represented by the Jones vector. Besides, two orthogonal Jones vectors form a polarization basis where any polarization state of a given electromagnetic wave can be expressed. If the Jones vectors of the incident and scattered waves are denoted by $\underline{\boldsymbol{E}}_\mathrm{I}$ and $\underline{\boldsymbol{E}}_\mathrm{S}$, respectively, with the far field assumption, the scattering process at a specific target can be represented as [4]

$$\underline{\boldsymbol{E}}_\mathrm{S} = \frac{\mathrm{e}^{-jkr}}{r} S \underline{\boldsymbol{E}}_\mathrm{I} = \frac{\mathrm{e}^{-jkr}}{r} \begin{bmatrix} S_{11} & S_{12} \\ S_{21} & S_{22} \end{bmatrix} \underline{\boldsymbol{E}}_\mathrm{I} \tag{1.1.14}$$

where $\dfrac{\mathrm{e}^{-jkr}}{r}$ accounts for the propagation effects both in amplitude and phase. $S = \begin{bmatrix} S_{11} & S_{12} \\ S_{21} & S_{22} \end{bmatrix}$ is the polarimetric scattering matrix and also called as the Sinclair scattering matrix.

For horizontal and vertical polarization basis (H, V), the polarimetric scattering matrix becomes

$$S = \begin{bmatrix} S_{\mathrm{HH}} & S_{\mathrm{HV}} \\ S_{\mathrm{VH}} & S_{\mathrm{VV}} \end{bmatrix} \tag{1.1.15}$$

where S_{HV} is the backscattered return from horizontal transmitting and vertical receiving polarization. Other terms are similarly defined.

The total scattering power *SPAN* is

$$SPAN = |S_{\mathrm{HH}}|^2 + |S_{\mathrm{HV}}|^2 + |S_{\mathrm{VH}}|^2 + |S_{\mathrm{VV}}|^2 \tag{1.1.16}$$

1.1.3 Polarization Basis Transformation

In order to understand and extract desired information from the scattering matrix, the transformation of polarization basis is needed to achieve a specific polarization combination. The (X,Y) polarization basis can be obtained from (H, V) polarization basis [3]

$$\begin{bmatrix} S_{\mathrm{XX}} & S_{\mathrm{XY}} \\ S_{\mathrm{YX}} & S_{\mathrm{YY}} \end{bmatrix} = \frac{1}{1+|\rho|^2} \begin{bmatrix} \mathrm{e}^{j\alpha} & 0 \\ 0 & \mathrm{e}^{-j\alpha} \end{bmatrix} \begin{bmatrix} 1 & \rho \\ -\rho^* & 1 \end{bmatrix} \begin{bmatrix} S_{\mathrm{HH}} & S_{\mathrm{HV}} \\ S_{\mathrm{VH}} & S_{\mathrm{VV}} \end{bmatrix} \begin{bmatrix} 1 & -\rho^* \\ \rho & 1 \end{bmatrix} \begin{bmatrix} \mathrm{e}^{-j\alpha} & 0 \\ 0 & \mathrm{e}^{j\alpha} \end{bmatrix} \tag{1.1.17}$$

where the polarization ratio is $\rho = \dfrac{\tan\phi + j\tan\tau}{1 - j\tan\phi\tan\tau}$ and ρ^* is the conjugate of ρ. The phase parameter is $\alpha = \tan^{-1}(\tan\phi\tan\tau)$. Besides, ϕ and τ are the geometric parameters of the polarization ellipse.

For the left and right circular polarization basis (L, R), $\rho = j$ and $\alpha = 0$ are valid. Then, the corresponding polarization is

$$\begin{aligned} \begin{bmatrix} S_{\mathrm{LL}} & S_{\mathrm{LR}} \\ S_{\mathrm{RL}} & S_{\mathrm{RR}} \end{bmatrix} &= \frac{1}{2} \begin{bmatrix} 1 & j \\ j & 1 \end{bmatrix} \begin{bmatrix} S_{\mathrm{HH}} & S_{\mathrm{HV}} \\ S_{\mathrm{VH}} & S_{\mathrm{VV}} \end{bmatrix} \begin{bmatrix} 1 & j \\ j & 1 \end{bmatrix} \\ &= \frac{1}{2} \begin{bmatrix} S_{\mathrm{HH}} + j(S_{\mathrm{HV}} + S_{\mathrm{VH}}) - S_{\mathrm{VV}} & j(S_{\mathrm{HH}} + S_{\mathrm{VV}}) + S_{\mathrm{HV}} - S_{\mathrm{VH}} \\ j(S_{\mathrm{HH}} + S_{\mathrm{VV}}) - S_{\mathrm{HV}} + S_{\mathrm{VH}} & -S_{\mathrm{HH}} + j(S_{\mathrm{HV}} + S_{\mathrm{VH}}) + S_{\mathrm{VV}} \end{bmatrix} \end{aligned} \tag{1.1.18}$$

For monostatic case (unless stated, the following discussions are always based on monostatic case), subject to the reciprocity condition ($S_{\mathrm{HV}} \approx S_{\mathrm{VH}}$), the elements of polarimetric scattering matrix with the circular polarization basis (L, R) are

$$\begin{aligned} S_{\mathrm{LL}} &= \frac{1}{2}(S_{\mathrm{HH}} - S_{\mathrm{VV}} + j2S_{\mathrm{HV}}), \quad S_{\mathrm{LR}} = S_{\mathrm{RL}} = \frac{j}{2}(S_{\mathrm{HH}} + S_{\mathrm{VV}}), \\ S_{\mathrm{RR}} &= \frac{1}{2}(S_{\mathrm{VV}} - S_{\mathrm{HH}} + j2S_{\mathrm{HV}}). \end{aligned} \tag{1.1.19}$$

1.1.4 Polarimetric Coherency Matrix in Linear Polarization Basis

In order to interpret scattering mechanism, a polarimetric scattering matrix can be projected into the Pauli spin matrices. For bistatic scattering case, the Pauli spin matrices are

$$P_1 = \frac{1}{\sqrt{2}}\begin{bmatrix} 1 & 0 \\ 0 & 1 \end{bmatrix}, P_2 = \frac{1}{\sqrt{2}}\begin{bmatrix} 1 & 0 \\ 0 & -1 \end{bmatrix}, P_3 = \frac{1}{\sqrt{2}}\begin{bmatrix} 0 & 1 \\ 1 & 0 \end{bmatrix} \quad \text{and} \quad P_4 = \frac{1}{\sqrt{2}}\begin{bmatrix} 0 & -j \\ j & 0 \end{bmatrix} \tag{1.1.20}$$

Then, the projection of polarimetric scattering matrix becomes

$$S = k_1 P_1 + k_2 P_2 + k_3 P_3 + k_4 P_4 \tag{1.1.21}$$

The coefficients $k_1 \sim k_4$ form the Pauli scattering vector, as

$$k_{\mathrm{P}_{(\mathrm{H,V})}} = \frac{1}{\sqrt{2}}[\, S_{\mathrm{HH}} + S_{\mathrm{VV}} \quad S_{\mathrm{HH}} - S_{\mathrm{VV}} \quad S_{\mathrm{HV}} + S_{\mathrm{VH}} \quad j(S_{\mathrm{HV}} - S_{\mathrm{VH}}) \,]^{\mathrm{T}} \tag{1.1.22}$$

For monostatic scattering case which satisfies the reciprocity condition, the Pauli spin matrices contain

$$P_1 = \frac{1}{\sqrt{2}}\begin{bmatrix} 1 & 0 \\ 0 & 1 \end{bmatrix}, P_2 = \frac{1}{\sqrt{2}}\begin{bmatrix} 1 & 0 \\ 0 & -1 \end{bmatrix} \quad \text{and} \quad P_3 = \frac{1}{\sqrt{2}}\begin{bmatrix} 0 & 1 \\ 1 & 0 \end{bmatrix} \tag{1.1.23}$$

The Pauli scattering vector becomes

$$k_{\mathrm{P}_{(\mathrm{H,V})}} = \frac{1}{\sqrt{2}}[\, S_{\mathrm{HH}} + S_{\mathrm{VV}} \quad S_{\mathrm{HH}} - S_{\mathrm{VV}} \quad 2S_{\mathrm{HV}} \,]^{\mathrm{T}} \tag{1.1.24}$$

The superiority of Pauli scattering vector representation lies in that it has the capability to directly indicate canonical scattering mechanism. For example, Pauli spin matrices P_1, P_2, and P_3 represent canonical odd-bounce scattering, double-bounce scattering, and volume scattering, respectively. In this vein, the elements in $k_{\mathrm{P}_{(\mathrm{H,V})}}$ indicate the scattering coefficients of these canonical scattering mechanisms accordingly.

With Pauli scattering vector, the second-order statistics of polarimetric coherency matrix T can be formed. Polarimetric coherency matrix inherits the representation advantage from the Pauli scattering vector, and it is defined as

$$T = \left\langle k_{\mathrm{P}_{(\mathrm{H,V})}} k^{\mathrm{H}}_{\mathrm{P}_{(\mathrm{H,V})}} \right\rangle = \begin{bmatrix} T_{11} & T_{12} & T_{13} \\ T_{21} & T_{22} & T_{23} \\ T_{31} & T_{32} & T_{33} \end{bmatrix}$$
$$= \frac{1}{2} \begin{bmatrix} \left\langle |S_{\mathrm{HH}} + S_{\mathrm{VV}}|^2 \right\rangle & \langle (S_{\mathrm{HH}} + S_{\mathrm{VV}})(S_{\mathrm{HH}} - S_{\mathrm{VV}})^* \rangle & \left\langle 2(S_{\mathrm{HH}} + S_{\mathrm{VV}}) S^*_{\mathrm{HV}} \right\rangle \\ \langle (S_{\mathrm{HH}} + S_{\mathrm{VV}})^* (S_{\mathrm{HH}} - S_{\mathrm{VV}}) \rangle & \left\langle |S_{\mathrm{HH}} - S_{\mathrm{VV}}|^2 \right\rangle & \left\langle 2(S_{\mathrm{HH}} - S_{\mathrm{VV}}) S^*_{\mathrm{HV}} \right\rangle \\ \langle 2(S_{\mathrm{HH}} + S_{\mathrm{VV}})^* S_{\mathrm{HV}} \rangle & \langle 2(S_{\mathrm{HH}} - S_{\mathrm{VV}})^* S_{\mathrm{HV}} \rangle & \left\langle 4|S_{\mathrm{HV}}|^2 \right\rangle \end{bmatrix} \tag{1.1.25}$$

where $\langle \cdot \rangle$ denotes the sample average, $k^{\mathrm{H}}_{\mathrm{P}_{(\mathrm{H,V})}}$ is the conjugate transpose of $k_{\mathrm{P}_{(\mathrm{H,V})}}$. T_{ij} is the (i,j) entry of T.

1.1.5 Polarimetric Covariance Matrix in Linear Polarization Basis

Polarimetric scattering matrix can be alternatively represented by another scattering vector which is named as the lexicographic scattering vector with each element of polarimetric scattering matrix as its entity. With the linear polarization basis (H, V) and the reciprocity condition, the lexicographic scattering vector is

$$k_{\mathrm{L}_{(\mathrm{H,V})}} = \begin{bmatrix} S_{\mathrm{HH}} & \sqrt{2} S_{\mathrm{HV}} & S_{\mathrm{VV}} \end{bmatrix}^{\mathrm{T}} \tag{1.1.26}$$

The corresponding second-order statistics of polarimetric covariance matrix $C_{(\mathrm{H,V})}$ is defined as

$$C_{(\mathrm{H,V})} = \left\langle k_{\mathrm{L}_{(\mathrm{H,V})}} k^{\mathrm{H}}_{\mathrm{L}_{(\mathrm{H,V})}} \right\rangle = \begin{bmatrix} \left\langle |S_{\mathrm{HH}}|^2 \right\rangle & \sqrt{2} \left\langle S_{\mathrm{HH}} S^*_{\mathrm{HV}} \right\rangle & \left\langle S_{\mathrm{HH}} S^*_{\mathrm{VV}} \right\rangle \\ \sqrt{2} \left\langle S^*_{\mathrm{HH}} S_{\mathrm{HV}} \right\rangle & 2 \left\langle |S_{\mathrm{HV}}|^2 \right\rangle & \sqrt{2} \left\langle S_{\mathrm{HV}} S^*_{\mathrm{VV}} \right\rangle \\ \left\langle S^*_{\mathrm{HH}} S_{\mathrm{VV}} \right\rangle & \sqrt{2} \left\langle S^*_{\mathrm{HV}} S_{\mathrm{VV}} \right\rangle & \left\langle |S_{\mathrm{VV}}|^2 \right\rangle \end{bmatrix} \tag{1.1.27}$$

The relationship between the Pauli and lexicographic scattering vectors is a unitary transform

$$k_{\mathrm{L}_{(\mathrm{H,V})}} = \frac{1}{\sqrt{2}} \begin{bmatrix} 1 & 1 & 0 \\ 0 & 0 & \sqrt{2} \\ 1 & -1 & 0 \end{bmatrix} k_{\mathrm{P}_{(\mathrm{H,V})}} = U_{\mathrm{P}_{(\mathrm{H,V})} 2 \mathrm{L}_{(\mathrm{H,V})}} k_{\mathrm{P}_{(\mathrm{H,V})}} \tag{1.1.28}$$

where $U_{\mathrm{P}_{(\mathrm{H,V})} 2 \mathrm{L}_{(\mathrm{H,V})}}$ is a unitary matrix.

Therefore, the link between polarimetric covariance matrix $C_{(\mathrm{H,V})}$ and polarimetric coherency matrix T is a similar transform

$$\begin{aligned} C_{(\mathrm{H,V})} &= U_{\mathrm{P}_{(\mathrm{H,V})}2\mathrm{L}_{(\mathrm{H,V})}} T U^{\mathrm{H}}_{\mathrm{P}_{(\mathrm{H,V})}2\mathrm{L}_{(\mathrm{H,V})}} = U_{\mathrm{P}_{(\mathrm{H,V})}2\mathrm{L}_{(\mathrm{H,V})}} T U^{-1}_{\mathrm{P}_{(\mathrm{H,V})}2\mathrm{L}_{(\mathrm{H,V})}} \\ &= \frac{1}{2}\begin{bmatrix} T_{11}+T_{22}+2\mathrm{Re}[T_{12}] & \sqrt{2}(T_{13}+T_{23}) & T_{11}-T_{22}-j2\mathrm{Im}[T_{12}] \\ \sqrt{2}(T_{13}+T_{23})^{*} & 2T_{33} & \sqrt{2}(T_{13}-T_{23})^{*} \\ T_{11}-T_{22}+j2\mathrm{Im}[T_{12}] & \sqrt{2}(T_{13}-T_{23}) & T_{11}+T_{22}-2\mathrm{Re}[T_{12}] \end{bmatrix} \end{aligned} \tag{1.1.29}$$

where $U^{-1}_{\mathrm{P}_{(\mathrm{H,V})}2\mathrm{L}_{(\mathrm{H,V})}}$ is the inverse of $U_{\mathrm{P}_{(\mathrm{H,V})}2\mathrm{L}_{(\mathrm{H,V})}}$, and $U^{-1}_{\mathrm{P}_{(\mathrm{H,V})}2\mathrm{L}_{(\mathrm{H,V})}} = U^{\mathrm{H}}_{\mathrm{P}_{(\mathrm{H,V})}2\mathrm{L}_{(\mathrm{H,V})}}$ for the unitary matrix.

1.1.6 Polarimetric Covariance Matrix in Circular Polarization Basis

Polarimetric covariance matrix with circular polarization basis is also commonly used for radar polarimetric data interpretation. In left and right $(\mathrm{L,R})$ circular polarization basis, with the reciprocity condition $(S_{\mathrm{LR}} \approx S_{\mathrm{RL}})$, from (1.1.19), the corresponding scattering vector $k_{\mathrm{L}_{(\mathrm{L,R})}}$ is

$$k_{\mathrm{L}_{(\mathrm{L,R})}} = \begin{bmatrix} S_{\mathrm{LL}} \\ \sqrt{2}S_{\mathrm{LR}} \\ S_{\mathrm{RR}} \end{bmatrix} = \frac{1}{2}\begin{bmatrix} S_{\mathrm{HH}}-S_{\mathrm{VV}}+j2S_{\mathrm{HV}} \\ j\sqrt{2}(S_{\mathrm{HH}}+S_{\mathrm{VV}}) \\ -(S_{\mathrm{HH}}-S_{\mathrm{VV}})+j2S_{\mathrm{HV}} \end{bmatrix} \tag{1.1.30}$$

The relationship between $k_{\mathrm{L}_{(\mathrm{L,R})}}$ and the Pauli scattering vectors is also a unitary transform

$$k_{\mathrm{L}_{(\mathrm{L,R})}} = \frac{\sqrt{2}}{2}\begin{bmatrix} 0 & 1 & j \\ j\sqrt{2} & 0 & 0 \\ 0 & -1 & j \end{bmatrix} k_{\mathrm{P}_{(\mathrm{H,V})}} = U_{\mathrm{P}_{(\mathrm{H,V})}2\mathrm{L}_{(\mathrm{L,R})}} k_{\mathrm{P}_{(\mathrm{H,V})}} \tag{1.1.31}$$

where $U_{\mathrm{P}_{(\mathrm{H,V})}2\mathrm{L}_{(\mathrm{L,R})}}$ is a unitary matrix.

The second-order statistics of polarimetric covariance matrix with circular polarization basis $(\mathrm{L,R})$ is

$$C_{(\mathrm{L,R})} = \left\langle k_{\mathrm{L}_{(\mathrm{L,R})}} k^{\mathrm{H}}_{\mathrm{L}_{(\mathrm{L,R})}} \right\rangle = \begin{bmatrix} \left\langle |S_{\mathrm{LL}}|^2 \right\rangle & \sqrt{2}\langle S_{\mathrm{LL}} S^*_{\mathrm{LR}} \rangle & \langle S_{\mathrm{LL}} S^*_{\mathrm{RR}} \rangle \\ \sqrt{2}\langle S^*_{\mathrm{LL}} S_{\mathrm{LR}} \rangle & 2\left\langle |S_{\mathrm{LR}}|^2 \right\rangle & \sqrt{2}\langle S_{\mathrm{LR}} S^*_{\mathrm{RR}} \rangle \\ \langle S^*_{\mathrm{LL}} S_{\mathrm{RR}} \rangle & \sqrt{2}\langle S^*_{\mathrm{LR}} S_{\mathrm{RR}} \rangle & \left\langle |S_{\mathrm{RR}}|^2 \right\rangle \end{bmatrix} \tag{1.1.32}$$

Therefore, the link between the polarimetric covariance matrix $C_{(\mathrm{L,R})}$ and polarimetric coherency matrix T is also a similar transform

$$C_{(\mathrm{L,R})} = U_{\mathrm{P}_{(\mathrm{H,V})}2\mathrm{L}_{(\mathrm{L,R})}} T U^{\mathrm{H}}_{\mathrm{P}_{(\mathrm{H,V})}2\mathrm{L}_{(\mathrm{L,R})}} = U_{\mathrm{P}_{(\mathrm{H,V})}2\mathrm{L}_{(\mathrm{L,R})}} T U^{-1}_{\mathrm{P}_{(\mathrm{H,V})}2\mathrm{L}_{(\mathrm{L,R})}} = \frac{1}{2} \begin{bmatrix} T_{22} + T_{33} + 2\mathrm{Im}[T_{23}] & \sqrt{2}(T_{13} + jT_{12})^* & T_{33} - T_{22} - j2\mathrm{Re}[T_{23}] \\ \sqrt{2}(T_{13} + jT_{12}) & 2T_{11} & \sqrt{2}(T_{13} - jT_{12}) \\ T_{33} - T_{22} + j2\mathrm{Re}[T_{23}] & \sqrt{2}(T_{13} - jT_{12})^* & T_{22} + T_{33} - 2\mathrm{Im}[T_{23}] \end{bmatrix} \tag{1.1.33}$$

where $U^{-1}_{\mathrm{P}_{(\mathrm{H,V})}2\mathrm{L}_{(\mathrm{L,R})}}$ is the inverse of $U_{\mathrm{P}_{(\mathrm{H,V})}2\mathrm{L}_{(\mathrm{L,R})}}$, and $U^{-1}_{\mathrm{P}_{(\mathrm{H,V})}2\mathrm{L}_{(\mathrm{L,R})}} = U^{\mathrm{H}}_{\mathrm{P}_{(\mathrm{H,V})}2\mathrm{L}_{(\mathrm{L,R})}}$ for the unitary matrix.

1.2 Polarimetric Radar Imaging

1.2.1 SAR Overview

The concept of synthetic aperture radar (SAR) was proposed by Carl Wiley of Goodyear Aerospace in 1951 [20, 21]. It was discovered that the Doppler information can be utilized to obtain high resolution in azimuth direction that is perpendicular to the beam illumination. Thereby, 2-D radar images are focused on the imaging scene. As a microwave imaging radar, SAR shows its superiority in remote sensing, since it can work day and night, and under almost all weather conditions. The first satellite SAR SEASAT was launched in 1978 which established the imaging radar as a practical remote sensing system from then on.

With the developed radar polarimetry theory and the progress in SAR, the combination of them as the PolSAR became a natural extension. This combination opened a new door for both radar polarimetry and microwave remote sensing. In 1985, the Jet Propulsion Laboratory successfully implemented the first practical fully polarimetric AIRSAR system [3]. It had unique capability to simultaneously acquire fully polarimetric data at three frequency bands (P-, L-, and C-band). These data sets were available to the radar community and promoted a large number of PolSAR data analysis and interpretation techniques. Later on, many airborne PolSAR systems came out. One of the representative systems is the Experimental SAR (E-SAR)

developed by the Microwaves and Radar Institute of the German Aerospace Research Centre (DLR). Besides, several advanced spaceborne PolSAR systems have been successfully launched recently. More detailed introductions and descriptions of these advanced PolSAR systems can be found in [3].

Besides, interferometric SAR (InSAR) was another development of the basic SAR from the baseline dimension. The first demonstration of InSAR capability was in 1974 by L. C. Graham [22]. A further step was the differential interferometry which can measure the deformation occurring during the several acquisitions. This technique was successfully demonstrated using SEASAT data sets by A. K. Gabriel et al. in 1989 [23]. Some reviews of InSAR techniques and advances can be found in [24–26].

Another milestone was achieved by the Shuttle SAR system SIR-C/X-SAR, which acquired multifrequency (X-, C-, and L-band) interferometric data in April and October, 1994. Fully polarimetric data sets at C- and L-band were also acquired during the second mission. Based on these datasets, S. Cloude and K. Papathanassiou proposed the innovative polarimetric SAR interferometry (PolInSAR) technique and demonstrated for forest height inversion via the investigation of polarization effect in SAR interferometry [27–29].

SAR obtains 2-D focused image by projecting the 3-D targets onto the 2-D imaging plane. InSAR has the ability to retrieve the target height by adding one more receiving antenna across the track. PolInSAR as a combination of PolSAR and InSAR can partially separate the scattering centers from different scattering mechanisms in the elevation direction. In order to reconstruct high-resolution 3-D image, similar to the synthetic aperture in azimuth direction, an aperture should be synthesized in the elevation direction as well, which leads to the concept of SAR tomography. The first demonstration of polarimetric SAR tomography with an airborne system was reported by A. Reigber and A. Moreira in 2000 [30, 31].

In order to get more information of the imaging scene, other data acquisition modes have been successfully demonstrated, such as multi-looking-aspect SAR [32], circular SAR [33], bistatic SAR [34]. In addition to airborne and spaceborne SAR systems, ground-based SAR system has also been developed and showed its flexibility for regional-scale monitoring [35, 36].

The general trends of advances in SAR imaging are: from single polarization to full polarization, from single frequency to multifrequency, from narrow frequency bandwidth to wide frequency bandwidth, from single baseline to multi-baseline. According to different applications, some other trends are also observed: from monostatic to bistatic, from single-looking-aspect to multi-looking-aspect. A review for these advancements is in [37].

1.2.2 SAR Imaging Principles

SAR is a microwave remote sensor usually deployed at a spaceborne or airborne platform. Comparing with optical sensors, SAR can work day and night, since it is